PNAS RESEARCH ARTICLE | APPLIED PHYSICAL SCIENCES

Brillouin super-cooling/heating in a non-Hermitian phononic dimer

Yicheng Zhu[a], Boyi Xue[a], Yuncong Sun[a], Qi Geng[a], Yuping Chen[b], Xianfeng Chen[b], Xiaoshun Jiang[c,1], Li Ge[d], and Wenjie Wan[a,b,1]

Affiliations are included on p. 7.

Edited by David Weitz, Harvard University, Cambridge, MA; received October 29, 2024; accepted April 8, 2025

The ability to coherently manipulate phonons through light permits cooling and heating microscale quantum systems for various critical fields in metrology, information processing, and sensing. However, these physical systems often are hard to isolate and open for exchanging energy externally, making themselves non-Hermitian. Here, we experimentally observe a super-cooling/heating state in a non-Hermitian phononic dimer, where the two independent phonon modes of distinct cooling/heating rates become synchronous in cooling/heating. Such super cooling/heating is manifested in a Parity–Time symmetric state controlled by two counterpropagating optical pumps. These results reveal the non-Hermitian nature of the phonon dimer and illustrate a coherent technique for synchronous cooling/heating non-Hermitian systems, paving the way for practical applications in quantum sensing and metrology.

non-Hermitian physics | Parity–Time symmetry | microcavity | Brillouin scattering | optomechanical cooling

Significance

Photon–phonon coupling plays a critical role in light–matter interaction. Reductions of phonons in specific modes (cooling) can be realized through anti-Stokes light scattering, a nonlinear up-conversion process by absorbing phonons. This ability to coherently manipulate phonons through light is critical for various fields in metrology, information processing, and sensing. However, phonons usually are not isolated in systems and are constantly exchanged with external modes; this constrains phonon cooling/heating efficiency. Here we experimentally observe super-cooling/heating states in a non-Hermitian phononic dimer, where two independent phonon modes of distinct cooling/heating rates become synchronous in Parity–Time symmetric state. These results pave ways for thermal management, optomechanical coherent control, and precision quantum metrology.

Cooling of mechanical motions remains a cornerstone for achieving exceptional sensitivity in high precision metrology (1–3), exploring the frontiers of quantum information processing (4–6), and probing the classical-to-quantum transition in macroscopic systems (7–9). Brillouin-based optomechanical cooling offers a unique path toward cooling phonons in optomechanical systems, complementing established laser cooling techniques for gases (10–13) and solids (14–16). Landmark demonstrations of forward Brillouin scattering in microcavities have allowed access to low frequency acoustical modes where phonon dissipation is lower than photons, allowing Brillouin cooling/heating of specific phonon modes through corresponding anti-Stokes/Stokes processes (17). Moreover, Inter-mode Brillouin cooling in a silicon waveguide has achieved a record 30 K reduction from room temperature for a phonon band (18). This approach opens exciting avenues for exploring quantum nonlinear optics (19), quantum computation (20, 21), and quantum networks (22–24) by leveraging broad optical and mechanical bandwidths.

However, a critical challenge limits further cooling/heating due to the phonon's interaction with the open environment, making the systems non-Hermitian (25). Among them, the simplest form of a dimer structure, also known as photonic/phononic molecule (26–29), permits energy exchange within the dimer, while individual gain/loss control of each phononic cavity leads to intriguing dynamics like phonon amplification (30), phonon laser (31, 32), and optomechanical cooling (33). More surprisingly, the competition between the internal coupling and the gain/loss control is composed of an emerging Parity–Time (PT) symmetry (34), enabling exotic behaviors of PT phonon laser (35), lasing at an exceptional point (EP) (32), and phononic dissipative coupling (36). Like its photonics counterpart, many of these prior works focus on the real eigenvalue solution to the non-Hermitian Hamiltonian, e.g., a degenerate supermode for a single mode phonon laser (32, 35), or mode splitting near an EP for enhanced sensing. However, less attention has been paid to the imaginary part of eigensolution (37). However, manipulating the imaginary part is essential for the optomechanical cooling/heating of ultranarrow linewidth Brillouin Lasers (38, 39), Superfluid Brillouin optomechanics (40), and continuous optomechanical waveguide (41). So far, the experimental demonstration of such optomechanical cooling has remained elusive in the non-Hermitian regime.

In this work, we experimentally demonstrate coherent and synchronous super-cooling/heating states in a PT symmetric phononic dimer, in which two counterpropagating phonon modes, i.e., clockwise (CW) and counterclockwise (CCW), are effectively coupled inside a Whispering-Gallery mode (WGM) type microcavity. A PT symmetry can be effectively realized in the dimer through nonlinear Brillouin scattering induced gain/loss, where two independently tunable optical pumps in two directions can individually control the directional phonon gain (Stokes) and loss (anti-Stokes). In this manner, the cooling/heating of phonons can be induced by the optical pumps through anti-Stokes

Author contributions: W.W. designed research; Y.Z., X.J., and L.G. performed research; B.X., Y.S., Q.G., Y.C., and X.C. analyzed data; and Y.Z., B.X., and W.W. wrote the paper.

The authors declare no competing interest.

This article is a PNAS Direct Submission.

[1]To whom correspondence may be addressed. Email: jxs@nju.edu.cn or wenjie.wan@sjtu.edu.cn.

This article contains supporting information online at https://www.pnas.org/lookup/suppl/doi:10.1073/pnas.2422355122/-/DCSupplemental.

Published May 12, 2025.

or Stokes Brillouin scattering, respectively. Meanwhile, by manipulating the CW/CCW pumping ratios, the two counter-propagating phonon modes experience a phase transition breaking the PT symmetry, where the two independent phonon modes, originally possessing distinct cooling/heating rates, become synchronous in the cooling/heating, i.e., super cooling/heating. Such simultaneous cooling/heating states govern the overall non-Hermitian dimer even at split phonon frequencies, given the effective energy transfer between the two modes. These results reveal the non-Hermitian nature of the acoustic phonon systems, indicate exotic dynamics due to the hidden phononic interaction, and pave the way for thermal management, optomechanical coherent control, and precision quantum metrology.

Results and Discussions

Microscale optical microcavities offer strong confinement and enhancement effects for both light and acoustic waves (42, 43). The optical microcavity is fabricated by arc-firing the tip of a silica fiber with a diameter of approximately 130 μm (Fig. 1*A*). Here, we excite an optical forward type Brillouin scattering in both directions inside a silica microsphere cavity to and realize a PT symmetric dimer of phonons in Fig. 1 (44, 27). A CW pump laser is launched from the left, coupling into the microsphere cavity via a tapered fiber. By resonantly coupled into a CW WGM, the CW pump can strongly induce an electrostriction effect, exciting nonlinear Brillouin scattering (BS). As a result, a strong acoustic phonon mode cycles in the CW direction. Meanwhile, a second CCW pump laser is injected oppositely from the other end of the fiber, generating another phonon mode in the CCW direction (Fig. 1*A*), effectively composing a phononic dimer. Here, the pump lasers are solely used to excite Brillouin scattering and provide gain for each phonon mode. Consequently, the CW/CCW pumps can individually control directional gains for phonons by adjusting the corresponding pump laser's intensities, which can be utilized for constructing a PT symmetry later.

Ideally, the CW and CCW acoustic modes are independent of each other. Due to the nonuniformity of material and structure in the actual system, symmetric breaking can occur. This disorder introduces scattering between modes, resulting in the coupling of acoustic modes in two directions. When the disorder induced scattering rate is low, an indirect coupling model can be used, which is the coupling of high-Q phonon modes with reverse low-Q phonon quasimode thermal bath (17), as in the case of ref. 45. When the disorder induced scattering rate is high, a direct coupling model can be used, which means that the high-Q phonon modes in two directions are directly coupled without the indirect effect of a large number of pseudo spin phonon modes of the same family. The use of direct coupling models can effectively explain the peculiar behavior of phonons in our work. In this manner, a PT symmetry can be constructed with directional BS gain and inherent phonon loss in such a phononic dimer (46–48). Fig. 1*B* illustrates such a PT symmetric dimer composed of the two opposite phonon modes, in which the pump's intensity differences can modulate the phonon modes, resulting in a lossy (blue) CW mode and a gain (red) CCW mode. Through the aforementioned internal coupling, the two phonon modes form the PT symmetric dimer (49, 50).

The cooling of phonons occurs when the pump light enters the anti-Stokes mode (Fig. 1*C*). In this process, a phonon and a photon of the pump are simultaneously absorbed, releasing a blue-shifted anti-Stokes photon (51, 52). Physically, the light exerts compressive pressure on the expanding acoustic wave, extracting energy from the acoustic field and causing the acoustic wave loss, this process is referred to the phonon cooling. Conversely, the heating of phonons can be achieved when the pump light enters the Stokes mode (Fig. 1*D*). In this case, the pump light releases a red-shifted Stokes photon along with an acoustic phonon, effectively providing gain for the phonon mode. As the light contracts the acoustic field, it applies pressure to the acoustic wave and transfers energy gain into it; this process is known as phonon heating. In both cases, the incident pump photons are annihilated, resulting in scattered photons with red-shifted Stokes frequencies or blue-shifted anti-Stokes frequencies. These scattering events either generate or annihilate phonons, causing the heating or cooling of phonons. Traditionally, the heating or cooling of mechanical modes is controlled by directly manipulating light radiation pressure. However, in our PT symmetric dimer system composed of phonons, the two acoustic modes are coupled together; this effectively introduces a second channel to provide gain or loss for the phonons, affecting the heating and cooling. By adjusting the pumps and cavity detunings, the phononic PT symmetric dimer can achieve synchronous

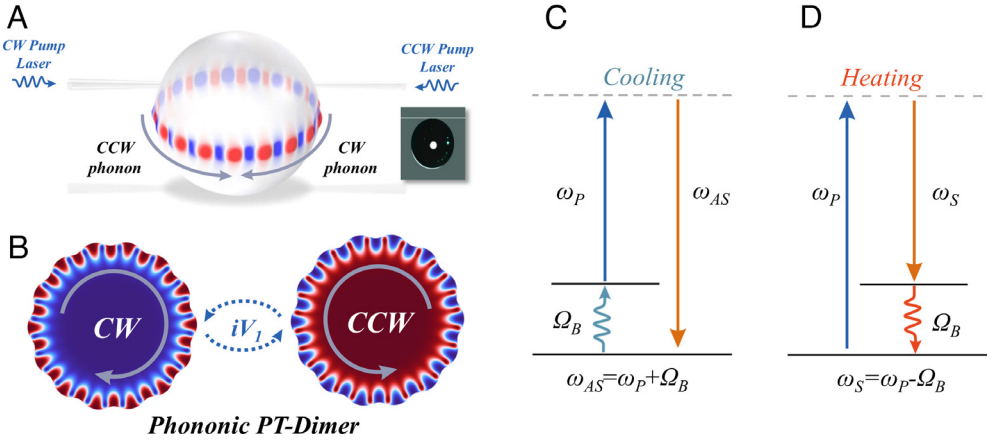

Fig. 1. Schematic diagram of super heating/cooling in a PT symmetric phononic dimer. (*A*) The model of bidirectional acoustic waves in microcavities. The pump light in CW and CCW directions is injected into the microcavity and coupled with the acoustic field in their respective directions through Brillouin scattering. Acoustic fields in two directions form standing waves and exhibit PT symmetry. The illustration on the *Right* is a photo of a microcavity under a microscope. The cross-sections of the acoustic field in two directions are shown in (*B*). Here, we present a scenario. Blue indicates the loss process for CW, while red indicates the gain process for CCW. The coupling between CW and CCW acoustic modes is achieved through a direct coupling coefficient V_1, forming a PT symmetric phonon dimer. Pump light absorbs phonon energy to produce high frequency anti-Stokes light. This is an acoustic energy loss process, therefore called cooling, as shown in the energy level diagram in (*C*). On the other hand, the pump light releases a phonon, producing low frequency Stokes light. This is a process of acoustic energy gain, called heating, as shown in (*D*).

cooling or heating rates in both directions despite their different pumping conditions; this phenomenon is termed super cooling/heating.

Like electromagnetic induced transparency in atoms, probe light can propagate without loss through destructive coherence between atomic energy levels, forming a transparent window. Nonlinear Brillouin scattering coupling can also lead to transparent or absorption peaks of the probe light in optical modes, known as Brillouin scattering induced transparency or absorption (49, 53, 54). Using the coupling wave equation, we conducted theoretical simulations and detailed analyses of the transmission spectra under different conditions in *SI Appendix*. And theoretical fitting curves (dashed line) can be obtained for the experimental data (solid line) in Figs. 3*A*–5*A* using the three-wave coupling equation. For convenience, we can express the high frequency anti-Stokes process and the low frequency Stokes process using the same set of equations. We have derived the theoretical analysis of Brillouin scattering induced transparency (BSIT) and Brillouin scattering induced absorption (BSIA) (53, 54) processes in detail in *SI Appendix*. Here, we can distinguish different processes by marking the symbol "±". H_- represents the anti-Stokes process and H_+ represents the Stokes process. For acoustic modes in two directions, we can obtain the non-Hermitian Hamiltonian:

$$H_{\pm}=\begin{pmatrix} \omega_{B0}-i\Gamma \pm i\dfrac{g_1^2}{\kappa} & V_1 \\ V_1 & \omega_{B0}-i\Gamma \pm i\dfrac{g_2^2}{\kappa} \end{pmatrix}, \qquad [1]$$

where ω_{B0} is intrinsic Brillouin frequency shift, Γ is intrinsic acoustic linewidth, g_1 and g_2 are the acoustic-optic coupling strength for CW and CCW, respectively, κ is optical mode linewidth, and V_1 is the direct coupling coefficient between acoustics. Under the condition of considering the pump light nondepletion approximation, we solve for the eigenvalue corresponding to the above non-Hermitian Hamiltonian, which is the eigenfrequency $\omega_{\pm}$ of the bidirectional acoustic fields corresponding to two processes:

$$\omega_{\pm}=\omega_{B0}-i\Gamma \mp i\frac{g_1^2+g_2^2}{2\kappa} \pm \frac{\sqrt{4\kappa^2 V_1^2-\Delta G^2}}{2\kappa}, \qquad [2]$$

where $\Delta G=g_1^2-g_2^2$, which represents the two pumps' coupling strength difference. It should be noted that the sign before the square root in Eq. **2** does not indicate two different processes (BSIT or BSIA). It indicates that there are two solutions after solving the square root, corresponding to the acoustic eigenfrequencies in two directions. The two directional acoustic fields constitute a typical non-Hermitian system. The eigenfrequencies, energy gain, or loss of two acoustic wave fields depend on the state of the system parameters. The equation after the square root includes real or imaginary numbers as well as EP. Therefore, according to Eq. **2**, changing the acousto-optic coupling strength difference in both directions can cause the system to undergo PT symmetric to broken PT phase.

For the case of super cooling, Fig. 2 presents the numerical results showing changes in the real and imaginary parts of the eigenfrequencies of two phonon modes during the anti-Stokes process (H_-). The real part represents the phonon frequencies, while the imaginary part corresponds to the linewidth, indicating energy loss. Here, we keep the power of the CCW pump light constant and gradually increase the CW pump light power, thereby increasing the phonon gain strength g_1 (with $g_1 > g_2$ and g_2 remaining constant, leading to an increase in $|\Delta G|$). As $|\Delta G|$ increases, the original phonons with different frequencies converge into a single frequency, and their originally identical linewidths begin to increase. Upon crossing the EP, the linewidths increase at different rates. The increase in linewidth indicates greater energy

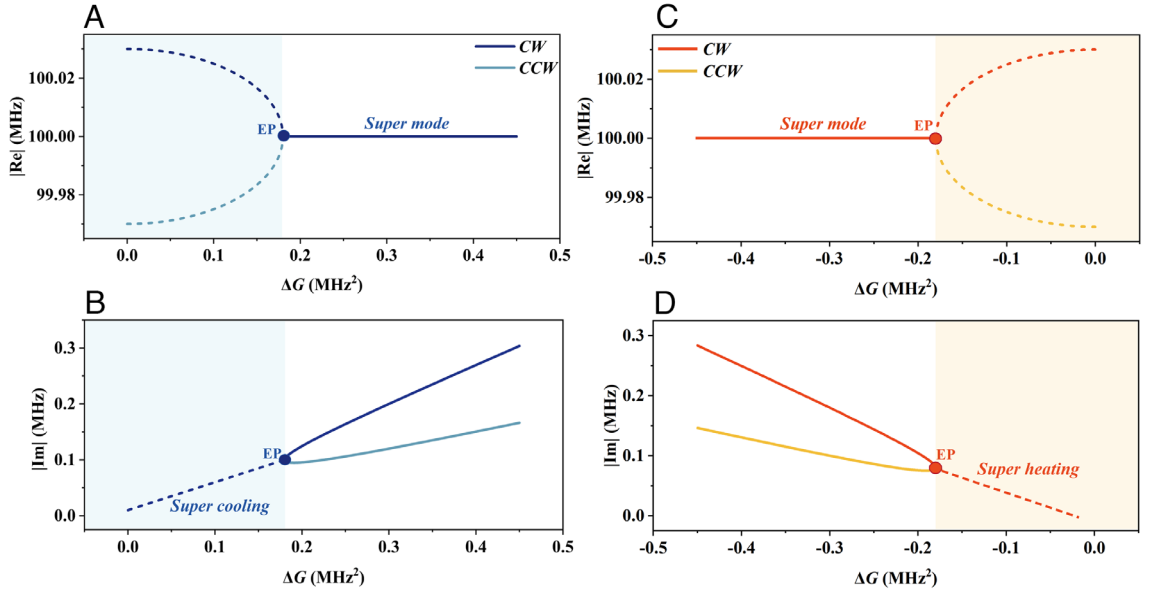

Fig. 2. Eigenfrequencies of the PT symmetric phononic dimer's non-Hermitian Hamiltonian: Real and imaginary parts of acoustic eigenfrequencies for CW and CCW varying with coupling strength difference. (*A* and *B*) are the real and imaginary parts of acoustic eigenfrequencies in the anti-Stokes process. The real part represents the acoustic frequency, and the imaginary part represents the linewidth. When the coupling strength g_1 increases ($g_2 < g_1$, and g_2 remains constant, $|\Delta G|$ increases), different acoustic frequencies are merged into one frequency. At the same time, the original linewidths increase. This indicates that anti-Stokes is a cooling process for the acoustic mode. Before passing through EP, the line widths in both directions increase synchronously, which is the supercooling state as shown by the blue dashed line. After passing through EP, two linewidths increase at different rates. The corresponding real acoustic frequencies are the same, which are two acoustic supermodes. (*C* and *D*) are the real and imaginary parts of acoustic eigenfrequencies in the Stokes process. As g_1 increases, the same acoustic frequencies split into different frequencies. The linewidths decrease with increasing g_1 ($g_2 > g_1$, and g_2 remains constant, $|\Delta G|$ decreases), indicating that this is a heating process for the acoustic mode. When crossing EP, the originally different line widths merge into the same linewidth and decrease together, corresponding to the superheating process.

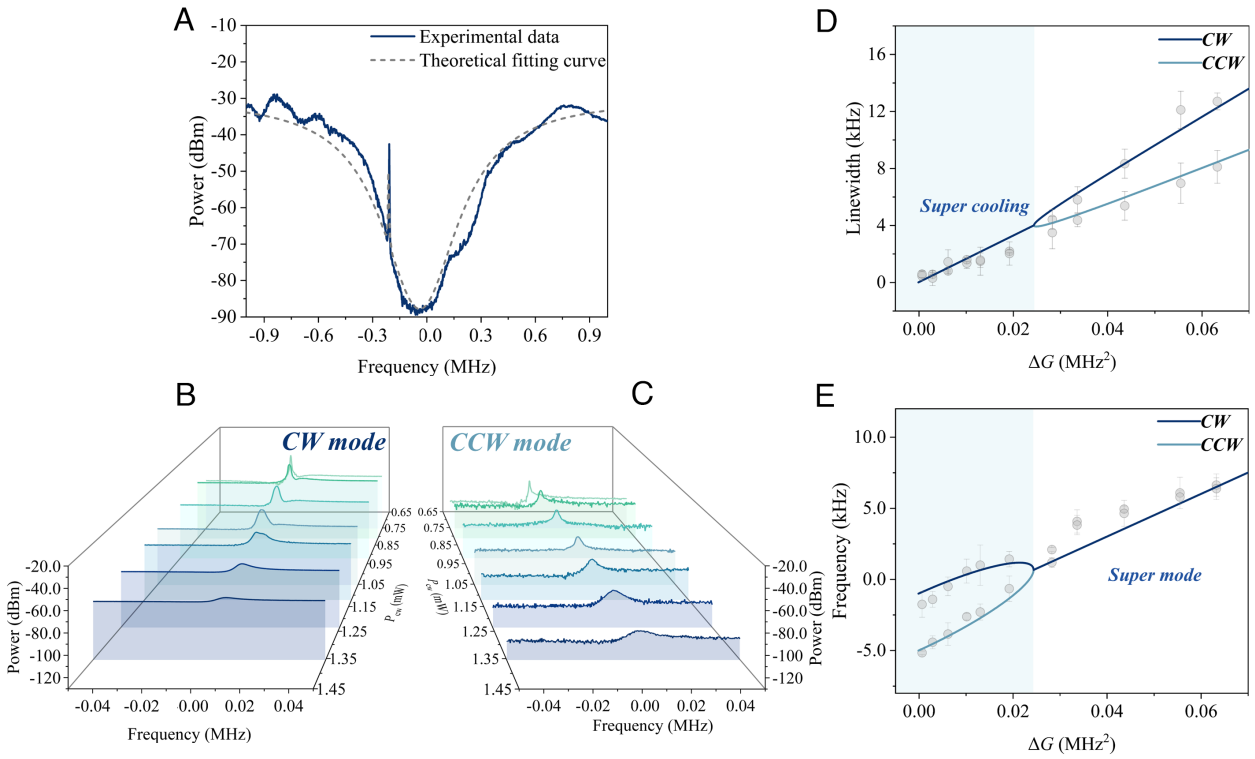

Fig. 3. Observation of supercooling in a phononic dimer. (*A*) Transmission spectrum of BSIT at high frequency anti-Stokes optical mode. Optical mode center is set to 0 MHz. The dash line represents the theoretical fitting curve by using the three-wave coupling equation. The solid line represents experimental results. Details can be found in *SI Appendix*. (*B* and *C*) are the BSIT transmission spectrums in two directions with the increase of CW pump power. (*D*) is CW and CCW acoustic linewidth and (*E*) is acoustic frequency. Gray dots represent experimental results. Solid lines represent theoretical fitting curves obtained from Eq. **2**. The splitting phonon modes under super cooling state merge and increase with the same linewidth. After crossing the EP, the splitting phonon modes merge into a supermode, and the linewidths split. Compared with different power functions, the linewidth and frequency experimental data satisfy the imaginary and real parts of the square root function of the Eq. **2** fitting curve very well. Details can be found in *SI Appendix*. As the power increases, the microcavity resonant frequency drifts due to the thermal locking effect, resulting in a frequency shift of the Brillouin signal obtained from frequency scanning.

dissipation, representing a cooling process. Before reaching the EP, the two phonon modes cool at the same rate, which is termed super cooling. In this regime, the system is in a PT symmetric state, corresponding to two distinct eigenfrequencies. After crossing the EP, the phonon modes cool at different rates despite sharing the same eigenfrequency, placing the system in a PT antisymmetric state. This state is also referred to as supermode (27, 55).

Moreover, for the superheating case, we have also conducted numerical simulations (Fig. 2 *C* and *D*) for the phonon modes of the Stokes process (H_+). As the phonon gain g_1 increases (with $g_1 < g_2$ and g_2 held constant, causing $|\Delta G|$ to decrease), a frequency difference emerges between the originally identical frequency acoustic waves. Additionally, their originally distinct linewidths decrease at varying rates. After crossing the EP, the line widths equalize and decrease synchronously. The reduction in linewidth indicates an increase in acoustic energy, signifying a heating process. Notably, as the phonon supermode passes through the EP, not only do the acoustic frequencies split, but the corresponding linewidths also decrease at the same rate. This synchronized reduction in linewidth reflects that both acoustic modes experience the same rate of energy gain, termed superheating. It should be noted that although both supercooling and heating occur in PT symmetric state, the entire system always maintains energy exchange with external inputs, which is a non-Hermitian physical system. It cannot be considered a purely Hermitian system. The dynamic characteristics of PT symmetric broken state or EP also play an important role. When the system is in PT symmetry broken state, different imaginary solutions of eigenvalues correspond to asynchronous heating or cooling between two phonon modes. This provides the possibility of manipulating specific mode heating or cooling.

Experimentally, we have observed the supercooling state of the phononic dimer in an anti-Stokes Brillouin scattering process. We select a high frequency anti-Stokes optical mode and observe a BSIT (53), as shown in Fig. 3*A*. The optical mode frequency shifts upward by 93.4 MHz, with a linewidth of approximately 0.14 MHz. The transparency peak, with a frequency detuning of about −0.2 MHz, appears on the left side of the optical mode. The dashed line represents a Lorentzian fit of the optical mode. The transparency peak is observed near the threshold, as the injected CW light power gradually increases from 0.27 mW to 1.54 mW, while the CCW pump power is fixed at 50 μW ($g_1 > g_2$, $\Delta G > 0$). Consequently, ΔG increases from 6.31×10^{-4} to 0.09 MHz^2. Fig. 3 *B* and *C* show the BSIT transmission spectra in both directions, while Fig. 3 *D* and *E* illustrate the variation of acoustic linewidth and acoustic frequency in both directions as ΔG changes. As ΔG increases, the initially identical acoustic linewidths increase synchronously. Upon crossing the EP at $\Delta G = 0.024$ MHz^2, the linewidths start to increase asynchronously at different rates. Before crossing the EP, the line widths are identical and increase at the same rate, indicating a supercooling state. The acoustic frequency behavior is the opposite: Initially, the two acoustic modes have distinct real eigenfrequencies. After crossing the EP, the frequencies converge, forming a supermode. The experimental results are consistent with theoretical predictions, but there are deviations. This deviation is mainly due to the interference of environmental thermal noise, such as laboratory temperature fluctuations or mechanical vibrations, in the measurement of phonon linewidth. By repeating the average experiment multiple times and carefully fixing the optical fibers and other equipment, this situation can be alleviated. Second, at the thermal noise limit, especially near EP, this deviation will also be amplified.

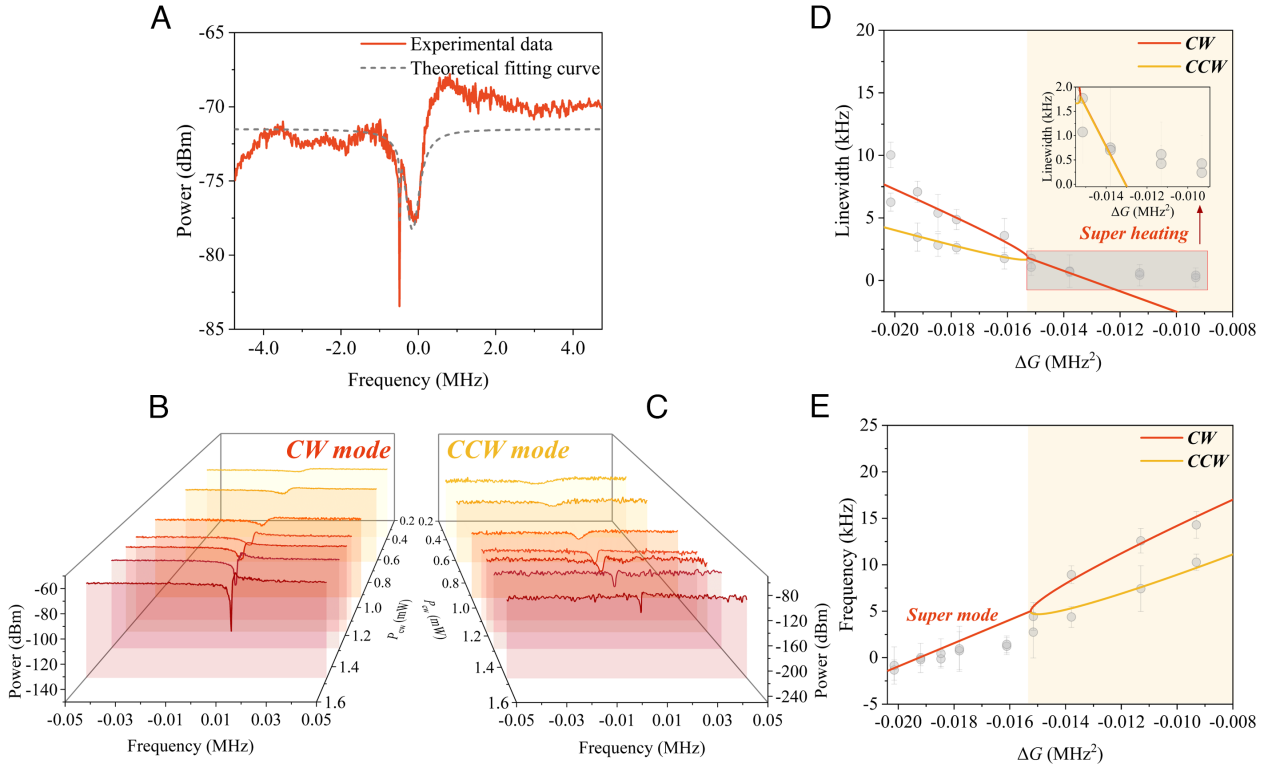

Fig. 4. Observation of superheating in a phononic dimer. (*A*) Transmission spectrum of BSIA at low frequency Stokes optical mode. Optical mode center is set to 0 MHz. The dashed line represents the theoretical fitting curve by using the three-wave coupling equation. The solid line represents experimental results. Details can be found in *SI Appendix*. (*B* and *C*) are the BSIA transmission spectrums in two directions with the increase of CW pump power. (*D*) is CW and CCW acoustic linewidth and (*E*) is acoustic frequency. Gray dots represent experimental results. Solid lines represent theoretical fitting curves obtained from Eq. **2**. The phonon modes under the supermode state have the same frequency and splitting linewidths. After crossing the EP, the linewidth of the splitting phonon modes under the superheating state merges and decreases. Compared with different power functions, the experimental data of linewidth and frequency, respectively, well satisfy the imaginary and real parts of the square root function of the Eq. **2** fitting curve. Details can be found in *SI Appendix*. Due to the thermal locking effect, Brillouin frequency signal obtained from frequency scanning shifts.

In the PT symmetry broken state, some gain is transferred from the CW mode to the CCW mode to compensate for the loss due to anti-Stokes cooling in the CCW direction. As a result, the phonon modes cool at different rates in the two directions. In the PT symmetric state, the energy spectrum has two real solutions, and the imaginary part reflects the same widened linewidth, which represents the supercooling state. The acoustic linewidth for the CW mode ranges from 0.58 kHz to 18.37 kHz, while for the CCW mode, it ranges from 0.46 kHz to 13.19 kHz. Gray dots represent experimental measurements, and solid lines correspond to theoretical calculations. In *SI Appendix*, we compared the fitting curves of two solutions under three different power functions with experimental data. The results show that the real and imaginary parts of the characteristic frequency under the square root function are most consistent with the experimental data. There is a significant difference between linear roots and cube roots. Therefore, it is reasonable to use the real and imaginary parts of the square root function of Eq. **2** to fit the frequencies and linewidths of phonon modes. In addition, manual measurement cannot perfectly capture the dynamic characteristics near EP, and experimental random errors result in unclear square root degeneracy features near EP in Figs. 3–5. By repeating the experiment three times in each group and adding error bars, the results still theoretically conform to the expected evolution trend from non-Hermitian PT symmetry state to PT symmetry broken state. Additional experimental details and data are available in *SI Appendix*.

Moreover, we have also realized the superheating state of the phononic dimer in a Stokes Brillouin scattering process. A low frequency Stokes mode is observed in Fig. 4*A*, where a BSIA (53) is located at a frequency shift of 316.16 MHz, with a linewidth of 0.59 MHz. In this case, we increased the CW pump power from 0.26 mW to 1.60 mW, while keeping the CCW pump power fixed at 4.3 mW ($g_1 < g_2$, $\Delta G < 0$). The corresponding ΔG changed from -0.0217 to -0.0093 MHz^2. Fig. 4 *B* and *C* display the BSIA transmission spectra in both directions. As ΔG increases (i.e., $|\Delta G|$ decreases), the acoustic linewidth in both directions decreases. Fig. 4 *D* and *E* present the extracted linewidth and acoustic frequency as functions of ΔG. Initially, the acoustic linewidth decreases at different rates in each direction. After crossing the EP, the system enters a superheating state, and the linewidths in both directions decrease synchronously. At this point, the acoustic frequencies are initially the same, indicating a supermode state. As ΔG increases, a frequency splitting occurs between the acoustic modes. The EP is reached at a CW pump power of 1.13 mW (ΔG = –0.0154 MHz^2).

In the supermode or PT symmetry broken state, the gain is transferred from the CW mode to the CCW mode, enhancing the Stokes heating in the CCW direction. Consequently, phonon modes heat at different rates in each direction. When the system is adjusted to the PT symmetric state, the energy spectrum solutions become two real values, and the imaginary part represents a compressed linewidth, indicating the superheating state. The linewidth for the CW mode decreases from 21.6 kHz to 0.24 kHz, while for the CCW mode, it decreases from 14.4 kHz to 0.43 kHz. Further experimental details and data can be found in *SI Appendix*.

More surprisingly, Fig. 5 shows that a chiral cooling and heating state can turn into a supercooling state after passing the EP in an anti-Stokes case. Similar to the previous supercooling case, a BSIT was found in an optical mode with a linewidth of 0.22 MHz with

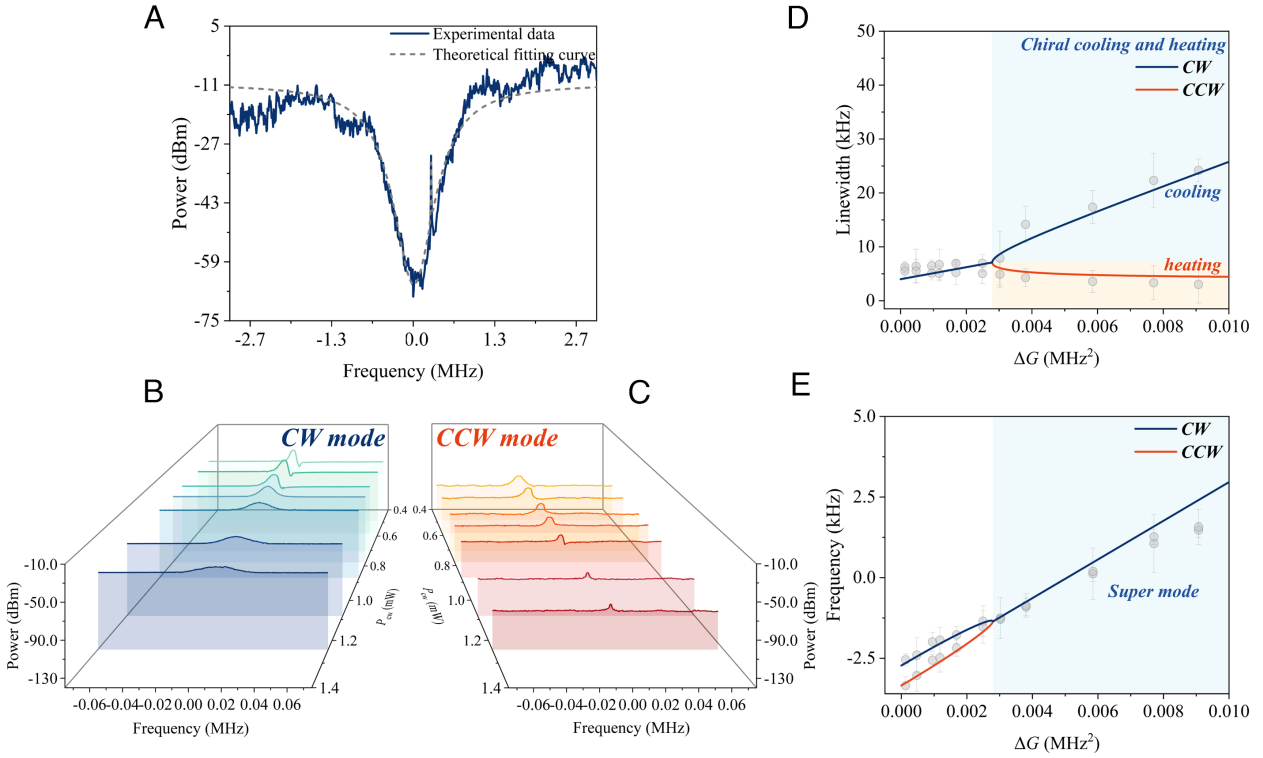

Fig. 5. Observation of phononic chiral cooling and heating. (*A*) Transmission spectrum of BSIT at high frequency anti-Stokes optical mode. Optical mode center is set to 0 MHz. The dashed line represents the theoretical fitting curve by using the three-wave coupling equation. The solid line represents experimental results. Details can be found in *SI Appendix*. (*B* and *C*) are the BSIT transmission spectrums in two directions with the increase of CW pump power. CCW power is 50% of CW. (*D*) is CW and CCW acoustic linewidth and (*E*) is acoustic frequency. Gray dots represent experimental results. Solid lines represent theoretical fitting curves obtained from Eq. **2**. The splitting phonon modes have the same linewidth. After crossing the EP, the splitting phonon modes merge into a supermode. However, the two phonon modes' linewidths split under the chiral cooling state, with one increasing and the other decreasing. Compared with different power functions, the linewidth and frequency experimental data satisfy the imaginary and real parts of the square root function of the Eq. **2** fitting curve very well. Details can be found in *SI Appendix*.

a frequency shift of 189.56 MHz. As shown in Fig. 5 *B* and *C*, the CW phonon mode linewidth increases after passing through EP, while the CCW phonon mode's linewidth decreases, by increasing the CW pump power and keeping the CCW pump power 50% of the CW's. Such evolution dynamics of eigenvalue's imaginary part (phonon's linewidth) and the real part (phonon's frequency) become more pronounced in Fig. 5 *D* and *E*. In the supercooling state, two phonon modes still possess distinct frequencies (Fig. 5*D*) similar to the previous case (Fig. 3); after passing through the EP when increasing the two pumps' contrast, the two phonon modes' frequencies merge into one supermode state uniformly.

Interestingly, for the imaginary part (Fig. 5*E*), the two phonon modes diverge from each other: The CW mode remains in a cooling state, however, the CCW mode turns into heating. In this supermode and PT symmetry broken state, the partial gain is transferred from the CW mode into the CCW one, compensating for its anti-Stokes cooling loss. This can be realized by reducing the difference between the two pumps. Moreover, the CCW mode must obtain sufficient gain from the CW mode to first overcome its own anti-Stokes cooling loss before heating can occur. In addition to its own anti-Stokes cooling loss, the CW mode also transfers a portion of energy to the CCW mode, exacerbating the cooling loss. Therefore, the results in Fig. 5*E* show that the heating rate of CCW mode is significantly lower than the cooling rate of CW mode. Analytically, this phenomenon can also be interpreted from Eq. **2**: The square root turns into two imaginary solutions with opposite signs, if the positive one under the root is greater than the negative imaginary part outside the root sign, this results in an overall positive imaginary part of the corresponding characteristic frequency, i.e., heating (more detailed derivation in supplement). Otherwise, both negative solutions of the two phonon modes correspond to both cooling cases as shown in Fig. 3. Among them, the variation of CW injection power is from 0.16 mW to 1.62 mW. The corresponding line width of CW varies from 6.26 kHz to 27.59 kHz. And the line width of CCW is from 5.51 kHz to 2.30 kHz. The specific details and data of the experiment can be obtained in *SI Appendix*.

Conclusions

In conclusion, we have constructed a PT dimer of phonons with two counter-propagating modes and observed a super-cooling/heating state in the dimer based on the absorption and release of phonon energy through Brillouin scattering.

Various optical cooling techniques (1, 2, 3, 7, 9) have been proposed and applied in the past few decades. However, traditional radiation pressure cooling typically relies on a single mechanical mode, which may lead to energy localization in single mode systems and make it difficult to simultaneously regulate heating and cooling in the same mechanical mode. This work can utilize PT symmetry to achieve directional distribution of phonon energy (as shown in Fig. 5). More importantly, by using phonon dimers, it is possible to effectively synchronize the cooling and heating of two phonon modes (Figs. 3 and 4), thereby achieving independent control of phonon modes on the same platform and providing higher operational flexibility.

Our experiments have demonstrated bidirectional phonon supercooling in high frequency anti-Stokes BSIT, as well as bidirectional phonon superheating in low frequency Stokes BSIA. By

manipulating the CW/CCW pumping ratios, the two counter-propagating phonon modes experience a phase transition breaking the PT symmetry, where the two independent phonon modes, originally possessing distinct cooling/heating rates, become synchronous in the cooling/heating, i.e., super cooling/heating. These results reveal the non-Hermitian nature of the acoustic phonon systems, the observed phonon–phonon interaction may open a door for a new paradigm of "phonon cooling" in condensed matter physics, which is crucial for many applications for microscale thermal management, optomechanical coherent control, and precision quantum metrology.

Materials and Methods

The continuous laser emitted by a 1,550 nm CTL (Toptica Photonics) with a narrow linewidth is divided into two paths at first. One path is the pump light in the CW direction, and the other path is the pump light in the CCW direction. Subsequently, the pump light in both directions can be modulated by EOM to produce sidebands that can be swept in both directions. Scanning frequency is used to observe the occurrence of high frequency anti-Stokes light (BSIT) or low frequency Stokes light (BSIA). The sweep signal is determined based on the RF signal provided by VNA (Siglent, SNA6032A). The pump light with sidebands in two directions is then passed through a tunable optical attenuator, to control the power difference between the two directions and create a difference in the coupling strength rate in both directions. By controlling the coupling rate difference between the two pumps, the state of phonon mode super-cooling/heating can be observed.

Data, Materials, and Software Availability. All study data are included in the article and/or *SI Appendix*.

ACKNOWLEDGMENTS. This work was supported by the National Key Research and Development Program (No. 2023YFA1407200; Grant No. 2023YFB3906400); the NSF of China (Grant No. 12274295, No.12341403).

Author affiliations: [a]State Key Laboratory of Photonics and Communications, University of Michigan-Shanghai Jiao Tong University Joint Institute, Shanghai Jiao Tong University, Shanghai 200240, China; [b]Department of Physics and Astronomy, Shanghai Jiao Tong University, Shanghai 200240, China; [c]National Laboratory of Solid State Microstructures, College of Engineering and Applied Science and School of Physics, Nanjing University, Nanjing 210093, China; and [d]Department of Physics and Astronomy, College of Staten Island, The City University of New York, New York, NY 10314

1. A. Geilen *et al.*, Extreme thermodynamics in nanolitre volumes through stimulated Brillouin-Mandelstam scattering. *Nat. Phys.* **19**, 1805–1812 (2023).
2. G. Bahl *et al.*, Brillouin cavity optomechanics with microfluidic devices. *Nat. Commun.* **4**, 1994 (2013).
3. Y. L. Zhang *et al.*, Enhanced optomechanical entanglement and cooling via dissipation engineering. *Phys. Rev. A* **101**, 063836 (2020).
4. H. Shin *et al.*, Control of coherent information via on-chip photonic–phononic emitter-receivers. *Nat. Commun.* **6**, 6427 (2015).
5. W. H. Renninger, P. Kharel, R. O. Behunin, P. T. Rakich, Bulk crystalline optomechanics. *Nat. Phys.* **14**, 601–607 (2018).
6. S. A. King *et al.*, Algorithmic ground-state cooling of weakly coupled oscillators using quantum logic. *Phys. Rev. X* **11**, 041049 (2021).
7. D. Kleckner, D. Bouwmeester, Sub-kelvin optical cooling of a micromechanical resonator. *Nature* **444**, 75–78 (2006).
8. P. D. Lett *et al.*, Observation of atoms laser cooled below the doppler limit. *Phys. Rev. Lett.* **61**, 169 (1988).
9. C. Samanta *et al.*, Nonlinear nanomechanical resonators approaching the quantum ground state. *Nat. Phys.* **19**, 1340–1344 (2023).
10. S. Stellmer, B. Pasquiou, R. Grimm, F. Schreck, Laser cooling to quantum degeneracy. *Phys. Rev. Lett.* **110**, 263003 (2013).
11. T. Langen *et al.*, Quantum state manipulation and cooling of ultracold molecules. *Nat. Phys.* **20**, 702–712 (2024).
12. S. Ruan *et al.*, Magneto-optical trap reaction microscope for photoionization of cold strontium atoms. *Phys. Rev. A* **109**, 023118 (2024).
13. K. M. O'Hara, S. L. Hemmer, M. E. Gehm, S. R. Granade, J. E. Thomas, Observation of a strongly interacting degenerate Fermi gas of atoms. *Science* **298**, 2179–2182 (2002).
14. J. Zhang *et al.*, Laser cooling of a semiconductor by 40 kelvin. *Nature* **493**, 504–508 (2013).
15. M. P. Hehlen *et al.*, First demonstration of an all-solid-state optical cryocooler. *Light Sci. Appl.* **7**, 15 (2018).
16. Y. Zhang *et al.*, Microwave mode cooling and cavity quantum electrodynamics effects at room temperature with optically cooled nitrogen-vacancy center spins. *NPJ Quantum Inf.* **8**, 125 (2022).
17. G. Bahl *et al.*, Observation of spontaneous Brillouin cooling. *Nat. Phys.* **8**, 203–207 (2012).
18. E. Kittlaus, N. Otterstrom, P. Rakich, On-chip inter-modal Brillouin scattering. *Nat. Commun.* **8**, 15819 (2017).
19. M. Tomes, F. Marquardt, G. Bahl, T. Carmon, Quantum-mechanical theory of optomechanical Brillouin cooling. *Phys. Rev. A* **84**, 063806 (2011).
20. S. Rips, M. J. Hartmann, Quantum information processing with nanomechanical qubits. *Phys. Rev. Lett.* **110**, 120503 (2013).
21. X. Y. Zhou *et al.*, Electrically interfaced Brillouin-active waveguide for microwave photonic measurements. *Nat. Commun.* **15**, 6796 (2024).
22. H. M. Doeleman *et al.*, Brillouin optomechanics in the quantum ground state. *Phys. Rev. Res.* **5**, 043140 (2023).
23. B. J. Eggleton *et al.*, Brillouin integrated photonics. *Nat. Photon.* **13**, 664–677 (2019).
24. H. Xu *et al.*, Nonreciprocal control and cooling of phonon modes in an optomechanical system. *Nature* **568**, 65–69 (2019).
25. J. Christensen, M. Willatzen, V. R. Velasco, M.-H. Lu, Parity-Time synthetic phononic media. *Phys. Rev. Lett.* **116**, 207601 (2016).
26. L. Ge, Effective size of a Parity-Time-symmetric dimer. *Phys. Rev. A* **109**, 023513 (2024).
27. B. Peng *et al.*, Parity–Time-symmetric whispering-gallery microcavities. *Nat. Phys.* **10**, 394–398 (2014).
28. H. Zhang *et al.*, Breaking anti-PT symmetry by spinning a resonator. *Nano Lett.* **20**, 7594–7600 (2020).
29. L. Feng, R. El-Ganainy, L. Ge, Non-Hermitian photonics based on Parity–Time symmetry. *Nat. Photon.* **11**, 752–762 (2017).
30. H. Wang *et al.*, Phonon amplification in two coupled cavities containing one mechanical resonator. *Phys. Rev. A* **90**, 053814 (2014).
31. I. S. Grudinin, H. Lee, O. Painter, K. J. Vahala, Phonon laser action in a tunable two-level system. *Phys. Rev. Lett.* **104**, 083901 (2010).
32. J. Zhang *et al.*, A phonon laser operating at an exceptional point. *Nat. Photon.* **12**, 479–484 (2018).
33. K. J. Vahala *et al.*, A phonon laser. *Nat. Phys.* **5**, 682–686 (2009).
34. C. Rüter *et al.*, Observation of Parity–Time symmetry in optics. *Nat. Phys.* **6**, 192–195 (2010).
35. H. Jing *et al.*, PT-symmetric phonon laser. *Phys. Rev. Lett.* **113**, 053604 (2014).
36. Q. Zhang, C. Yang, J. Sheng, H. Wu, Dissipative coupling-induced phonon lasing. *Proc. Natl. Acad. Sci. U.S.A.* **119**, e2207543119 (2022).
37. J. Hou *et al.*, Enhanced frequency conversion in Parity-Time symmetry line. *Phys. Rev. Lett.* **132**, 256902 (2024).
38. M.–G. Suh, Q. F. Yang, K. J. Vahala, Phonon-limited-linewidth of Brillouin lasers at cryogenic temperatures. *Phys. Rev. Lett.* **119**, 143901 (2017).
39. W. Loh *et al.*, Cooling of an integrated Brillouin laser below the thermal limit. *Opt. Express* **30**, 22562–22571 (2022).
40. A. Kashkanova *et al.*, Superfluid Brillouin optomechanics. *Nat. Phys.* **13**, 74–79 (2017).
41. N. T. Otterstrom, R. O. Behunin, E. A. Kittlaus, P. T. Rakich, Optomechanical cooling in a continuous system. *Phys. Rev. X* **8**, 041034 (2018).
42. Y. Chen *et al.*, Exceptional points with memory in a microcavity Brillouin laser. *Optica* **9**, 971–979 (2022).
43. Y. Zhu *et al.*, Storing light near an exceptional point. *Nat. Commun.* **15**, 8101 (2024).
44. C. M. Bender, S. Boettcher, Real spectra in non-Hermitian Hamiltonians having PT symmetry. *Phys. Rev. Lett.* **80**, 5243 (1998).
45. S. Kim *et al.*, Dynamically induced robust phonon transport and chiral cooling in an optomechanical system. *Nat. Commun.* **8**, 205 (2017).
46. Şk. Özdemir, S. Rotter, F. Nori, L. Yang, Parity–Time symmetry and exceptional points in photonics. *Nat. Mater.* **18**, 783–798 (2019).
47. S. Soleymani *et al.*, Chiral and degenerate perfect absorption on exceptional surfaces. *Nat. Commun.* **13**, 599 (2022).
48. M. Peng *et al.*, Nonreciprocal slow or fast light in anti-symmetric optomechanics. *Phys. Rev. A* **107**, 033507 (2023).
49. F. Zhang, Y. Feng, X. Chen, L. Ge, W. Wan, Synthetic anti-PT symmetry in a single microcavity. *Phys. Rev. Lett.* **124**, 053901 (2020).
50. J. Hou *et al.*, Enhanced frequency conversion in Parity-Time symmetry line. *Phys. Rev. Lett.* **132**, 256902 (2024).
51. Y.-S. Park, H. Wang, Resolved-sideband and cryogenic cooling of an optomechanical resonator. *Nat. Phys.* **5**, 489–493 (2009).
52. Z. Shen, Y. Zhang, C. Zou, G. Guo, C. Dong, Dissipatively controlled optomechanical interaction via cascaded photon-phonon coupling. *Phys. Rev. Lett.* **126**, 163604 (2021).
53. J. Kim, M. C. Kuzyk, K. Han, H. Wang, G. Bahl, Non-reciprocal Brillouin scattering induced transparency. *Nat. Phys.* **11**, 275–280 (2015).
54. T. Qin *et al.*, Fast- and slow-light-enhanced light drag in a moving microcavity. *Commun. Phys.* **3**, 118 (2020).
55. J. Zhang *et al.*, A phonon laser operating at an exceptional point. *Nat. Photon.* **12**, 479–484 (2018).